THE JOURNAL OF PHYSICAL CHEMISTRY B
A JOURNAL OF THE AMERICAN CHEMICAL SOCIETY

pubs.acs.org/JPCB

Article

Characterizing Fast Conformational Exchange of Aromatic Rings Using Residual Dipolar Couplings: Distinguishing Jumplike Flips from Other Exchange Mechanisms

Matthias Dreydoppel, Mikael Akke, and Ulrich Weininger*

Cite This: J. Phys. Chem. B 2022, 126, 7950–7956

Read Online

ACCESS | Metrics & More | Article Recommendations

ABSTRACT: Aromatic ring flips are a hallmark of protein dynamics. They are experimentally studied by NMR spectroscopy, where recent advances have led to improved characterization across a wide range of time scales. Results on different proteins have been interpreted as continuous diffusive ring rotations or jumplike flips, leading to diverging views of the protein interior as being fluidlike or solidlike, respectively. It is challenging to distinguish between these mechanisms and other types of conformational exchange because chemical-shift-mediated line broadening provides only conclusive evidence for ring flips only if the system can be moved from the slow- to intermediate/fast-exchange regime. Moreover, whenever the chemical shift difference between the two symmetry-related sites is close to zero, it is not generally possible to determine the exchange time scale. Here we resolve these issues by measuring residual dipolar coupling (RDC)-mediated exchange contributions using NMR relaxation dispersion experiments on proteins dissolved in dilute liquid crystalline media. Excellent agreement is found between the experimental difference in RDC between the two symmetry-related sites and the value calculated from high-resolution X-ray structures, demonstrating that dynamics measured for F52 in the B1 domain of protein G reports on distinct, jumplike flips rather than other types of conformational exchange.

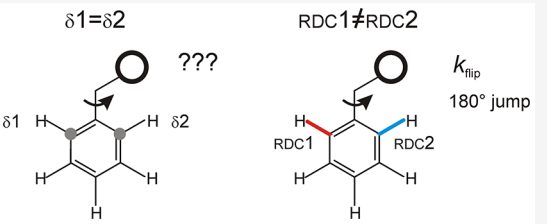

INTRODUCTION

Conformational dynamics of proteins is essential for biological function. Aromatic ring flips, i.e., 180° rotations of the χ_2 dihedral angle in Phe and Tyr side chains, are a hallmark of transient conformational fluctuations in proteins.[1,2] Aromatic side chains in the interior of globular proteins commonly undergo rapid rotations, as gauged by the observation of a single peak in the NMR spectrum originating from the two symmetry related nuclei of the ring. In the past, ring flip rates have been measured for only a limited number of proteins by using line shape analysis or longitudinal exchange experiments.[1,3−6] The development of site-selective isotope labeling schemes for aromatic side chains[7−14] has enabled relaxation dispersion experiments for aromatic ^{13}C and ^{1}H sites[15−18] and led to a renaissance in studying ring flips by NMR spectroscopy.[19−25]

The rotation of an aromatic side chain located inside the protein core requires that the surrounding side chains transiently create sufficient volume to accommodate the ring rotation. Temperature- and pressure-dependent experiments make it possible to determine the activation enthalpy ($\Delta H^{\ddagger}$), entropy ($\Delta S^{\ddagger}$), and volume ($\Delta V^{\ddagger}$) of this process.[1,5,20,21,26,27] Recently, we presented a combined analysis of temperature- and pressure-dependent ring flip data that enabled us to also determine the change in compressibility ($\Delta\kappa^{\ddagger}$) between ground and transition states of a ring flip,[19] which indicates that the transition state is liquidlike, whereas the ground state is solidlike. This result differs from conclusions reached in another study of the dynamics of surface-exposed aromatic residues in ubiquitin, which suggest that the ground state is liquidlike and the aromatic rings undergo continuous diffusive rotations.[24] Thus, further studies are warranted to provide detailed insights into the mechanism and energetics of aromatic ring dynamics and how these properties might differ among aromatic side chains located in different environments, e.g., in the protein core or closer to the protein surface.

To date, the study of ring flips by solution-sate NMR spectroscopy has mainly relied on measuring exchange contributions to the line width (or longitudinal exchange for very slow cases), caused by differences in the chemical shifts of the symmetry-related pairs of ^{1}Hδ, ^{1}Hε, ^{13}Cδ, or ^{13}Cε nuclei. However, it is not uncommon that none of these sites display significant differences in chemical shift, thereby making ring flip studies by NMR relaxation difficult or impossible.[20,22,28] Furthermore, when separate peaks cannot be observed for the

Received: July 19, 2022
Revised: August 3, 2022
Published: September 30, 2022

two sides of the aromatic ring, it has been impossible to determine with certainty that exchange broadening is due to ring flips rather than other types of conformational exchange.

Here we demonstrate that these impediments can be resolved by studying exchange broadening mediated by residual dipolar couplings,[29,30] introduced by partial alignment of the protein in dilute liquid crystalline media.[31] The use of RDC-mediated conformational exchange is particularly powerful in the case of aromatic ring flips because the approach resolves cases where the chemical shift difference is (close to) zero and, importantly, provides critical structural information to distinguish whether aromatic rings undergo distinct, jumplike flips, or continuous diffusive ring rotation as invoked recently,[24] or other types of conformational exchange.

MATERIALS AND METHODS

Protein Expression and Purification. The 1-^{13}C and 2-^{13}C glucose-labeled B1 domain of Staphylococcal protein G (GB1; UniProtKB P06654) carrying the mutations T2Q, N8D, and N37D (QDD-GB1) was expressed and purified as described elsewhere.[32] It has been established that QDD-GB1 has the same structure as wild-type GB1 and that comparisons between the two variants are valid;[32] henceforth, we refer to the triple mutant simply as GB1. 1-^{13}C glucose labeling results in site-selective ^{13}C enrichment at the δ positions of Phe and Tyr residues, while 2-^{13}C glucose labeling results in site-selective ^{13}C enrichment at their ε positions.[10,12,14]

NMR Sample Preparation. To induce weak alignment of the protein in the static magnetic field, samples were prepared by using dilute liquid crystalline phases consisting of hexaethylene glycol monododecyl ether ($C_{12}E_6$, Sigma) and *n*-hexanol (Fluka), which were used without further purification. $C_{12}E_6$ was dissolved in the protein solution (2.3 mM of 1-^{13}C or 3.3 mM of 2-^{13}C glucose labeled GB1) in H_2O containing 10% D_2O to reach a $C_{12}E_6$/water ratio of 8 wt %.[33] The pH was adjusted to 7.0, followed by addition of *n*-hexanol to a $C_{12}E_6$/*n*-hexanol molar ratio of 0.64. The alcohol was added in microliter steps under vigorous mixing and shaking of the solution at a temperature of 35 °C. After cooling below 10 °C, the solution became opalescent and stably monophasic and was stored at 4 °C. Aqueous GB1 samples were dissolved to a concentration of 1 mM in 20 mM HEPES, 90% H_2O/10% D_2O, with small amounts of NaN_3. The pH was adjusted to 7.0 in the sample.

NMR Spectroscopy. All experiments were performed at a static magnetic field strength of 14.1 T. Experiments on the 1-^{13}C glucose-labeled sample were performed on a Bruker Avance IV spectrometer equipped with a cryoprobe, while RDC measurements on the 2-^{13}C glucose-labeled sample were performed on a Bruker Avance III spectrometer equipped with a room temperature probe. Aromatic L-optimized TROSY-selected ^{13}C $R_{1\rho}$ relaxation dispersion experiments[16] were performed with the spin-lock placed on-resonance with F52δ at temperatures of 5, 10, and 15 °C. In short, the pulse sequence selects the TROSY component by using an S^3E element,[34] and the relaxation period is divided into two blocks separated by a S^3CT selective inversion element.[35] In each relaxation block,^{13}C magnetization was aligned along the B_1 field axis by using a 4 ms tan/tanh adiabatic ramp,[36] spin-locked on-resonance using spin-lock field strengths of $\omega_1/2\pi$ = {923, 1259, 1688, 2048, 2610, 3784, 4313, 5486} Hz, and finally returned to the original state by a time-reversed adiabatic ramp. Two separate experiments were acquired with and without the spin-lock relaxation period for each effective field, from which relaxation rate constants were calculated as $R_{1\rho} = \ln(I_{rlx}/I_{ref})/t_{rlx}$, where I_{rlx} and I_{ref} are the intensities measured in the spectra acquired with and without the relaxation period, respectively, and t_{rlx} = 20 ms is the length of the relaxation period. Relaxation dispersion data were acquired as an interleaved pseudo-3D experiment, where the effective field strengths were varied prior to incrementing the indirect evolution period t_1.

Relaxation Data Analysis. NMR spectra were processed with NMRPipe[37] and analyzed with PINT.[38] The on-resonance $R_{1\rho}$ relaxation rate constant is the sum of the intrinsic transverse relaxation rate constant and the exchange contribution: $R_{1\rho} = R_{2,0} + R_{ex}$. Miloushev and Palmer have derived a general expression for symmetric two-state exchange[39] that is applicable to the case of aromatic ring flips, which involves fixed populations, $p_a = p_b = 0.5$. In the present case, where the spin-lock is applied on-resonance with the average signal, the exchange contribution can be expressed as

$$R_{ex} = \frac{k}{2} - \frac{k}{2}\sqrt{1 - \frac{\Delta\omega^2}{\frac{\omega_a^2\omega_b^2}{\omega_1^2} + k^2\left[1 - \frac{\Delta\omega^2}{4}\frac{\omega_a^2 + \omega_b^2}{\omega_a^2\omega_b^2 + k^2\omega_1^2}\right]}} \quad (1)$$

where $\Delta\omega$ is the difference in resonance frequency between the two sites, ω_a and ω_b are the effective field strengths at the resonance frequency of each site (i.e., $\omega_a^2 = ((\omega_{a,RDC}/2 + \Omega_a)^2 + \omega_1^2)$, and vice versa for ω_b), Ω_a is the chemical shift (Larmor frequency) offset from the carrier, $\omega_{a,RDC}$ is the RDC, ω_1 is the spin-lock field strength (all expressed in units of rad/s), and $k = 2k_{flip}$, with k_{flip} being the ring flip rate. Data sets were fitted simultaneously, while imposing the restrictions $k_{flip}(T_{high}) > k_{flip}(T_{low})$ and $R_{2,0}(T_{high}) \leq R_{2,0}(T_{low})$.[20] In addition, the restriction $\Delta\omega(T_{high}) < \Delta\omega(T_{low})$ was used, which takes into account the reduced alignment strength at higher temperatures.[33] T_{high} and T_{low} denote the sample temperatures of the relaxation dispersion experiments. Errors in the fitted parameters were estimated by using Monte Carlo simulations.[40]

RDC Measurements and Structure-Based Predictions. Backbone $^{13}C^{\alpha}-^{1}H^{\alpha}$ RDCs and aromatic $^{13}C-^{1}H$ RDCs were measured in non-decoupled, non-constant time $^{1}H-^{13}C$ HSQC spectra, with and without alignment medium, at 5 °C. RDCs were measured for 11 clearly resolved cross-peaks corresponding to sites T17α, T18α, A26α, K31α, W43(α,η2,ε3,ζ2,ζ3), T51α, and F52α. The resulting RDCs were used to calculate the alignment tensors (AT) based on the 1.92 and 1.14 Å X-ray crystal structures (PDB entities 1PGB[41] and 2GI9,[42] respectively), with the program REDCAT,[43] provided in NMRbox.[44] In REDCAT five independent RDCs in combination with the proteins structure are sufficient for AT calculation.[43] Its robustness was checked by systematically excluding each of the 11 RDCs, leading to the same results within margin of error. Aromatic RDCs in Tyr and Phe residues were predicted based on the experimentally determined AT and the crystal structures. Errors in the predicted RDCs were estimated as one standard deviation of RDCs predicted from 200 replicate REDCAT calculations.

The difference between the $^{1}H-^{13}C$ RDC values predicted for the individual symmetry-related sites (δ1 and δ2) can be

https://doi.org/10.1021/acs.jpcb.2c05097
J. Phys. Chem. B 2022, 126, 7950−7956

compared with the value ($\Delta\omega_{RDC}$) determined experimentally from the RDC-mediated relaxation dispersion data

$$\Delta\omega_{RDC} = |\omega_{\delta1,RDC} - \omega_{\delta2,RDC}|/2 \quad (2)$$

The factor 1/2 arises because only one-half of the RDC affects the TROSY line, while the other half affects the anti-TROSY line. The absolute value arises from $\Delta\omega^2$ (see eq 1). The averaged value of the RDC measured in the spectrum is given by

$$\langle\omega_{RDC}\rangle = (\omega_{\delta1,RDC} + \omega_{\delta2,RDC})/2 \quad (3)$$

RDCs for $\delta1$ and $\delta2$ were calculated as a function of the χ_2 dihedral angle, as follows. Using both the 1PGB and 2GI9 structures, the atomic coordinates of the F52 aromatic ring were updated following stepwise rotation by 2° around the C_β−C_γ−C_ζ axis, while keeping all other atom coordinates constant. The PDB coordinates were saved after each step to cover in total a rotation of 360°. On the basis of these hypothetical, intermediate state structures and the previously calculated AT, ^{13}C−^{1}H RDCs were calculated by using REDCAT for each of the 180 different χ_2 dihedral angles.

RESULTS AND DISCUSSION

In isotropic solutions, aromatic ring flips of Phe and Tyr residues can normally be studied only if they possess different chemical shifts in the two δ or ε positions; although in special cases it can be possible to measure ring flips rates even if the shifts are identical.[22] In total, there are four sites to study: ^{13}Cδ and ^{13}Cε (Figure 1A) and ^{1}Hδ and ^{1}Hε (Figure 1B). Because

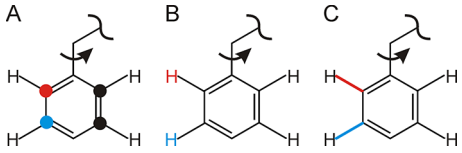

Figure 1. Differences in resonance frequencies between the two symmetry-related positions of the aromatic ring enable measurement of ring flip rates: (A) ^{13}C chemical shifts differ between the colored and black carbon nuclei; (B) ^{1}H chemical shifts differ between the colored and black hydrogen nuclei; (C) RDCs differ between the colored and black ^{1}H−^{13}C moieties. The δ and ε positions are colored red and blue, respectively.

of the narrow chemical shift range of aromatic nuclei and the strong coupling between them, relaxation dispersion experiments require site-selective ^{13}C labeling to probe the carbons[7,10−14] and additional ^{2}H labeling of vicinal sites to probe the protons.[15,18,45] It is not uncommon that only a subset of the four sites can be studied, either because the chemical shifts of the two symmetric positions of the ring are identical or because a site is severely broadened by exchange under the desired experimental conditions. In GB1 the chemical shifts have been measured for three aromatic residues under slow exchange conditions induced by low temperature and high pressure.[20] Y3 displays chemical shift differences for all four sites: ^{1}Hδ, ^{13}Cδ, ^{1}Hε, and ^{13}Cε. F30 displays chemical shift differences for ^{1}Hδ, ^{13}Cδ, and ^{1}Hε, with the δ position being severely broadened throughout the permissible temperature range from 1 °C to the onset of unfolding at 40 °C. F52 only displays chemical shift differences for ^{13}Cε, but not for the other nuclei.

Here we take advantage of the fact that the RDC usually differs between the two sides of the ring (Figure 1C). By studying RDC-mediated exchange line broadening using relaxation dispersion methods, we increase the number of possible probes for characterizing ring flips from four to six (i.e., four chemical shifts plus two RDCs). Moreover, RDCs allow for a direct structural interpretation, which is rarely possible based on chemical shifts, except in cases where the chemical shift difference between the symmetry-related sites has been measured under slow exchange conditions. We used F52 ^{13}Cδ as a critical test case because the $\delta1$ and $\delta2$ carbons have identical chemical shifts ($\Delta\omega_{iso}$ = 0) and therefore yield flat ^{13}C relaxation dispersion profiles in isotropic solutions (Figure 2A).

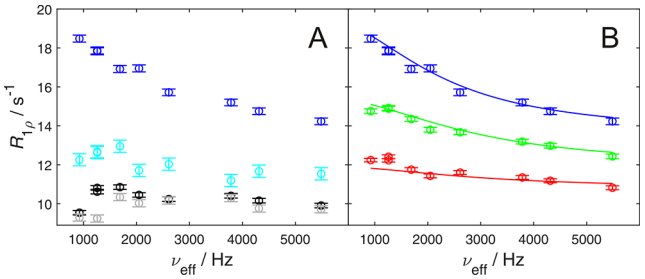

Figure 2. Relaxation dispersion profiles for F52 ^{13}Cδ and Y33 ^{13}Cδ. Data were recorded using on-resonance spin-lock fields at a static magnetic field strength of 14.1 T. (A) Relaxation dispersion profiles acquired at 5 °C in aqueous buffer (F52 in cyan and Y33 in gray) and $C_{12}E_6$/*n*-hexanol liquid crystalline alignment medium (F52 in blue and Y33 in black). (B) Relaxation dispersion profiles acquired in alignment medium at temperatures of 5 °C (blue, as in panel A), 10 °C (green), and 15 °C (red). The continuous lines represent the fitted symmetric two-state exchange model (eq 1).

RDC-Mediated Exchange Line Broadening Studied by ^{13}C $R_{1\rho}$ Relaxation Dispersion. Aromatic ^{13}C $R_{1\rho}$ relaxation experiments performed on F52δ in $C_{12}E_6$/*n*-hexanol liquid crystalline medium[33] reveals a significant dispersion profile, even though the ^{13}C chemical shift difference is zero,[20] as also evidenced by a flat dispersion profile in isotropic solvent (Figure 2A). In contrast, Y33δ, which undergoes fast ring flips, displays flat dispersion profiles independent from the alignment medium. This result directly points to a significant difference in RDC between the two symmetry-related positions of the aromatic ring that enables a reliable fit of exchange rates (Figure 2B).

Fitting eq 1 to the experimental data yields exchange rates that agree well with previously determined values obtained from ^{13}C $R_{1\rho}$ data for the F52ε position (Table 1), thereby validating RDC-mediated exchange as a method to study

Table 1. Ring Flip Rates of F52δ Determined by RDC-Enabled ^{13}C $R_{1\rho}$ Relaxation Dispersion Experiments

T (°C)	k_{flip} ^{13}Cδ RDC (10^3 s^{-1})	k_{flip} ^{13}Cε[a] (10^3 s^{-1})	$\Delta\omega_{RDC}$ (Hz)	$\langle\omega_{RDC}\rangle$ (Hz)
5	6.9 ± 1.5	7.8 ± 1.0	90 ± 7	12 ± 1
10[b]	8.7 ± 1.8	8.5 ± 0.8	78 ± 9	8 ± 1
15	9.0 ± 6.2	10.2 ± 0.7	45 ± 10	5 ± 1

[a]Derived from ref 19. [b]Identical results were obtained on a sample of 1 mM protein concentration: k_{ex} = (8.8 ± 3.0) × 10^3 s^{-1} and $\Delta\omega_{RDC}$ = 74 ± 8 Hz.

https://doi.org/10.1021/acs.jpcb.2c05097
J. Phys. Chem. B 2022, 126, 7950−7956

aromatic ring flips. The relaxation dispersion profiles are more pronounced at lower temperatures (Figure 2B), in agreement with the expectation that decreased rates of ring flipping lead to greater exchange contributions to $R_{1\rho}$ (cf. eq 1). In addition, the alignment is weaker at higher temperature, leading to reduced $R_{1\rho}$ as a consequence of reduced $\Delta\omega_{RDC}$, as can also be seen from the lower average RDC value, $\langle\omega_{RDC}\rangle$, measured in the $^{1}H-^{13}C$ HSQC spectrum (Table 1).

Unfortunately, none of the other aromatic residues in GB1 are amenable to RDC-mediated exchange characterization for the following reasons: Y3 has the lowest $\Delta\omega_{RDC}$ value and displays significant differences in isotropic ^{13}C chemical shifts ($\Delta\omega_{iso}$ = 210 and 316 Hz at 14.1 T), which renders the contribution from the RDC-mediated broadening relatively small; Y33 is surface exposed and exhibits very fast ring flips; and F30 and Y45 are severely broadened at conditions optimal for $R_{1\rho}$ experiment. The latter three cases represent general challenges in studying ring flips that are independent of the RDC approach. In fact, our approach should be widely applicable to aromatic residues suitable for characterization by relaxation dispersion experiments because $\Delta\omega_{RDC}$ is expected to be sufficiently large in the majority of cases. As an example, we calculated $\Delta\omega_{RDC}$ values for all δ and ε positions of the Tyr and Phe residues in GB1, based on the crystal structure and the determined alignment tensor. The predicted $\Delta\omega_{RDC}$ values range between 46 and 97 Hz, which are large enough to produce significant relaxation dispersion profiles provided that the exchange rate falls in a suitable regime. For comparison, these $\Delta\omega_{RDC}$ values correspond to ^{13}C chemical shift differences of 0.3 and 0.65 ppm at a magnetic field strength of 14.1 T. In rare cases the $^{1}H-^{13}C$ bond vectors of both symmetry-related sites might be aligned identically with respect to the laboratory frame, which would yield $\Delta\omega_{RDC}$ near zero. This problem can be circumvented by choosing an alignment medium that generates a different alignment tensor. Otherwise, we expect that RDC-mediated exchange line broadening will serve as a valuable probe of aromatic side chain dynamics.

To validate the fitted $\Delta\omega_{RDC}$ values, we plotted the temperature-dependent data against $\langle\omega_{RDC}\rangle$, which indeed shows the expected linear correlation (Figure 3) (cf. eqs 2 and 3). By taking the linear combinations of $\Delta\omega_{RDC}$ and $\langle\omega_{RDC}\rangle$, we extract $\omega_{\delta1,RDC}$ = 102 ± 7 Hz and $\omega_{\delta2,RDC}$ = −78 ± 7 Hz. These RDCs can be compared with values predicted from crystal structures, which provides insights into the mechanism of ring rotations, as described below.

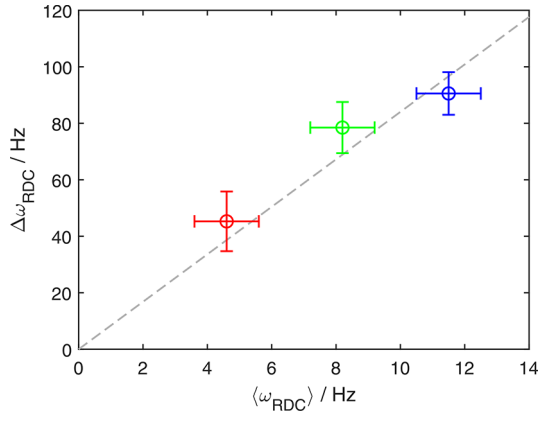

Figure 3. Validation of $\Delta\omega_{RDC}$ values extracted from ^{13}C $R_{1\rho}$ relaxation dispersion data. Fitted $\Delta\omega_{RDC}$ values are plotted against $\langle\omega_{RDC}\rangle$ measured in the non-decoupled $^{1}H-^{13}C$ HSQC spectra at 5 °C (blue), 10 °C (green), and 15 °C (red). The dashed line is a linear fit with zero intercept drawn to show the expected linearity.

RDC Values Determined by Relaxation Dispersion Agree with Predictions from Crystal Structures. We interpreted the fitted $\Delta\omega_{RDC}$ values and $\langle\omega_{RDC}\rangle$ determined at 5 °C in structural terms. We first determined the alignment tensor of GB1 from the experimental RDC values and two high-resolution crystal structures, 1PGB[41] (1.92 Å) and 2GI9[42] (1.14 Å), using REDCAT.[43] On the basis of the structural coordinates and the resulting alignment tensors, we then predicted the $^{1}H-^{13}C$ RDC values for the individual symmetry-related sites, $\omega_{\delta1,RDC}$ and $\omega_{\delta2,RDC}$, of F52δ1 and F52δ2. The experimental and predicted RDCs are compared in Table 2. Excellent agreement is observed between the predicted and experimental values of $\Delta\omega_{RDC}$ and $\langle\omega_{RDC}\rangle$ when comparing with the 1PGB crystal structure. The 2GI9 structure shows slightly less good agreement, particularly for$\omega_{\delta2,RDC}$, while the agreement for $\Delta\omega_{RDC}$ is still reasonable.

Table 2. Experimental and Predicted RDC Values for F52δ at 5 °C[a]

	$\omega_{\delta1,RDC}$	$\omega_{\delta2,RDC}$	$\Delta\omega_{RDC}$	$\langle\omega_{RDC}\rangle$
experiment	102 ± 7	−78 ± 7	90 ± 7	12 ± 1
1PGB	100 ± 2	−83 ± 2	91 ± 2	9 ± 2
2GI9	102 ± 3	−97 ± 3	99 ± 2	2 ± 2

[a]Units in Hz.

Importantly, the agreement between the experimental results for F52δ and the RDCs predicted from the orientations of the H−C vectors in the crystal structure clearly indicates that the observed exchange is caused by aromatic ring flips, rather than other types of conformational exchange, such as exchange between alternative ring orientations induced by changes in the χ_1 dihedral angle. While large-scale χ_1 fluctuations are not expected to occur readily for aromatic side chains that are packed tightly in the protein core, such as F52 in GB1, this type of motion is possible for solvent exposed residues. Thus, quantitative measurement of RDC-mediated exchange makes it possible to conclusively identify ring flip dynamics even for aromatic residues that undergo fast exchange on the chemical shift time scale under all attainable experimental conditions.

It should be noted that the present evidence for jumplike ring flips does not suggest that the ring does not undergo ground-state fluctuations within each rotamer well. However, the correlation times of intrawell fluctuations are expected to be much shorter (faster) than the correlation times of ring flips, which are rare events in the case of buried rings in the interior of proteins. There is a difference of approximately 10^5 between these correlation times (sub-ns and 0.1 ms in the present case). Thus, the intrawell fluctuations are completely averaged prior to each ring flip, and the ring-flip rate extracted from the relaxation dispersion data is governed by the difference between the population-weighted ground-state and transition-state free energies.

RDC-Mediated Exchange Line-Broadening Provides Evidence for Distinct Jumplike Ring Flips. It has been proposed that aromatic rings in ubiquitin undergo complete ring rotation by continuous diffusion rather than jumplike flips.[24] The distinction between jumplike flips and such "continuous diffusion" has not previously been investigated

https://doi.org/10.1021/acs.jpcb.2c05097
J. Phys. Chem. B 2022, 126, 7950−7956

more directly by liquid-state NMR. Here we address this issue by comparing how the effective value of $\Delta\omega_{RDC}$ differs between the two scenarios.

We predicted the variation in RDC values as a function of the χ_2 dihedral angle (Figure 4). To estimate $\Delta\omega_{RDC}$ and

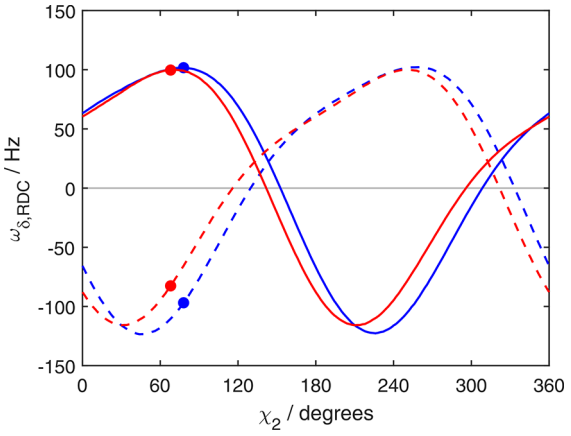

Figure 4. Predicted RDC values as a function of the χ_2 dihedral angle of F52δ at 5 °C. $\omega_{\delta1,RDC}$ and $\omega_{\delta2,RDC}$ plotted vs χ_2 as solid and dashed lines, respectively, based on the X-ray structures 1PGB (red) and 2GI9 (blue). Ground-state values are indicated as filled dots.

$\langle\omega_{RDC}\rangle$ values resulting from continuous diffusive motion around χ_2, we averaged each of the two $\omega_{\delta,RDC}$ values over a complete 360° rotation by using either a uniform probability distribution (which is rather unphysical) or a probability distribution weighted by the χ_2 dihedral potential of the CHARMM36 force field with the bottom of the potential well set to either the nominal value of χ_2 = 90° or the actual value measured in the crystal structure, χ_2 = 68° (1PGB) or χ_2 = 78° (2GI9), before calculating $\Delta\omega_{RDC}$ and $\langle\omega_{RDC}\rangle$.

Neither the uniform nor the weighted distribution is expected to accurately portray reality because the probability distribution of ring orientations will surely depend also on tertiary interactions in the protein core. However, the greater the distinguishing features of the probability distribution, the less likely is continuous diffusional rotation. Thus, the two different averaging procedures employed here provide a first reasonable comparison of our experimental results with those expected from the continuous diffusion model. The resulting values of $\Delta\omega_{RDC}$ and $\langle\omega_{RDC}\rangle$ are listed in Table 3. As might be expected, the continuous diffusion model yields significantly reduced $\Delta\omega_{RDC}$ values near zero,[46] quite different from the experimental result of $\Delta\omega_{RDC}$ = 90 Hz. By contrast, the $\Delta\omega_{RDC}$ value calculated from the ground-state structure shows excellent agreement with the value determined by experiment. In addition, $\langle\omega_{RDC}\rangle$ is underestimated by the continuous

Table 3. Predicted RDC Values for F52δ at 5 °C (in Hz), Averaged over a Complete 360° Rotation around χ_2

	$\Delta\omega_{RDC}$		$\langle\omega_{RDC}\rangle$	
crystal structure	1PGB	2GI9	1PGB	2GI9
uniform probability	0.4	0.5	5.3	5.2
weighted probability[a]	0.3	0.4	9.4	6.7
weighted probability[b]	0.3	0.4	6.0	4.8

[a]Dihedral potential with minimum at χ_2 = 90°. [b]Dihedral potential with minimum at χ_2 = 68° (1PGB) or χ_2 = 78° (2GI9).

diffusion model. Taken together, these results provide strong evidence that the aromatic ring of F52 in GB1 undergoes a distinct, jumplike 180° flip around the χ_2 dihedral angle.

Solid-state NMR spectroscopy can provide powerful information about aromatic ring dynamics because the dipolar coupling strength and asymmetry parameter depend on the underlying motional modes.[46−49] We note that a previous solid-state NMR study of microcrystalline wild-type GB1 indicated that the F52 ring is nearly rigid in this environment,[48] which is clearly not the case in solution as demonstrated herein. Thus, the breathing motions that enable the F52 ring to flip are apparently quenched in the crystalline state. These differences highlight the critical role of the protein packing density, where not only the local environment around the ring is important but also more remote interactions such as the protein−protein interface of the crystal.

Structural Aspects of a Ring Flips. We have previously determined the activation parameters of the F52 ring flip, including $\Delta H^{\ddagger}$ and $\Delta S^{\ddagger}$, as well as the activation volume, $\Delta V^{\ddagger}$, and the isothermal volume compressibility.[19] These parameters present a consistent picture of the transition state as being significantly expanded with fewer stabilizing interactions than the ground state, while populating a larger number of conformations and having a compressibility similar to that of unfolded proteins, indicating that the F52 ring flip is made possible by relatively large-scale breathing motions that resemble local unfolding.[19] Yet, our present results are fully consistent with a jumplike two-state exchange process that does not involve any intermediate or off-pathway high-energy conformations. This result contrasts with recent observations involving a buried tyrosine residue in an SH3 domain,[50] which exchanges between the ground state and an alternative high-energy conformation characterized by different values of the χ_2 dihedral angle. MD simulations showed that local breathing motions create a significant void volume ($\Delta V^{\ddagger}$ = 65 Å^3) allowing for rapid ring flips (k_{flip} > 25000 s^{-1}). However, once in a while (70 s^{-1}) the ring flip is apparently intercepted by interactions with surrounding residues, leading to recompaction of the local structure and trapping of the ring in the high-energy conformation, which consequently is off-pathway with respect to the ring flip reaction. X-ray crystal structures of variant SH3 domains that stabilize the high-energy state provide unique structural details of large-scale structural changes that might be coupled to ring flipping.[50]

The difference in behavior observed for the aromatic residues in the SH3 domain,[50] ubiquitin,[24] and GB1 illustrates the complexity and variation among proteins in the intramolecular dynamics associated with ring flipping, which evidently is critically dependent on local structure and interactions.

CONCLUSIONS

We have shown that RDC-mediated exchange line broadening enables measurement of aromatic ring flip dynamics using relaxation dispersion experiments. As reported previously for other nuclei,[29,30] the approach offers a valuable complement to experiments probing exchange mediated by the isotropic chemical shift. In the special case of aromatic side chains, the experimentally determined RDCs provide particularly powerful information about the mechanism of the ring flips by making it possible to distinguish between distinct jumps and alternative models, including continuous diffusive motion around the χ_2 dihedral angle as proposed by Wand and co-workers based on

https://doi.org/10.1021/acs.jpcb.2c05097
J. Phys. Chem. B 2022, 126, 7950−7956

studies of aromatic residues in ubiquitin.[24] We conclude that the aromatic side chain of F52 in GB1 undergoes distinct, jumplike ring flips, in full agreement with our previous conclusions based on temperature- and pressure-dependent studies of the activation volume and transition state compressibility of the exchange process.[19]

AUTHOR INFORMATION

Corresponding Author

Ulrich Weininger − *Institute of Physics, Biophysics, Martin-Luther-University Halle-Wittenberg, D-06120 Halle (Saale), Germany;* orcid.org/0000-0003-0841-8332; Phone: +49 345 55 28555; Email: ulrich.weininger@physik.uni-halle.de

Authors

Matthias Dreydoppel − *Institute of Physics, Biophysics, Martin-Luther-University Halle-Wittenberg, D-06120 Halle (Saale), Germany*

Mikael Akke − *Division of Biophysical Chemistry, Center for Molecular Protein Science, Department of Chemistry, Lund University, SE-22100 Lund, Sweden;* orcid.org/0000-0002-2395-825X

Complete contact information is available at: https://pubs.acs.org/10.1021/acs.jpcb.2c05097

Notes

The authors declare no competing financial interest.

ACKNOWLEDGMENTS

This work was supported by Deutsche Forschungsgemeinschaft (WE 5587/1-2), the Swedish Research Council (2018-4995), and the ERASMUS+ programme. This study made use of NMRbox: National Center for Biomolecular NMR Data Processing and Analysis, a Biomedical Technology Research Resource (BTRR), which is supported by NIH Grant P41GM111135 (NIGMS).

REFERENCES

(1) Wagner, G.; Demarco, A.; Wüthrich, K. Dynamics of Aromatic Amino-Acid Residues in Globular Conformation of Basic Pancreatic Trypsin-Inhibitor (Bpti).1. H-1 Nmr-Studies. *Biophys. Struct. Mech.* **1976**, *2* (2), 139−158.

(2) Wüthrich, K. The way to NMR structures of proteins. *Nat. Struct. Biol.* **2001**, *8* (11), 923−925.

(3) Campbell, I. D.; Dobson, C. M.; Williams, R. J. P. Proton Magnetic-Resonance Studies of Tyrosine Residues of Hen Lysozyme-Assignment and Detection of Conformational Mobility. *Proc. Royal Soc. B* **1975**, *189* (1097), 503−509.

(4) Baturin, S. J.; Okon, M.; McIntosh, L. P. Structure, dynamics, and ionization equilibria of the tyrosine residues in Bacillus circulans xylanase. *J. Biomol. NMR* **2011**, *51* (3), 379−394.

(5) Hattori, M.; Li, H.; Yamada, H.; Akasaka, K.; Hengstenberg, W.; Gronwald, W.; Kalbitzer, H. R. Infrequent cavity-forming fluctuations in HPr from Staphylococcus carnosus revealed by pressure- and temperature-dependent tyrosine ring flips. *Protein Sci.* **2004**, *13* (12), 3104−3114.

(6) Nall, B. T.; Zuniga, E. H. Rates and Energetics of Tyrosine Ring Flips in Yeast Iso-2-Cytochrome-C. *Biochemistry* **1990**, *29* (33), 7576−7584.

(7) Kasinath, V.; Valentine, K. G.; Wand, A. J. A C-13 Labeling Strategy Reveals a Range of Aromatic Side Chain Motion in Calmodulin. *J. Am. Chem. Soc.* **2013**, *135* (26), 9560−9563.

(8) Lichtenecker, R. J. Synthesis of aromatic C-13/H-2-alpha-ketoacid precursors to be used in selective phenylalanine and tyrosine protein labelling. *Organic & Biomolecular Chemistry* **2014**, *12* (38), 7551−7560.

(9) Lichtenecker, R. J.; Weinhaupl, K.; Schmid, W.; Konrat, R. alpha-Ketoacids as precursors for phenylalanine and tyrosine labelling in cell-based protein overexpression. *J. Biomol. NMR* **2013**, *57* (4), 327−331.

(10) Lundström, P.; Teilum, K.; Carstensen, T.; Bezsonova, I.; Wiesner, S.; Hansen, D. F.; Religa, T. L.; Akke, M.; Kay, L. E. Fractional C-13 enrichment of isolated carbons using [1-C-13]- or [2-C-13]-glucose facilitates the accurate measurement of dynamics at backbone C-alpha and side-chain methyl positions in proteins. *J. Biomol. NMR* **2007**, *38* (3), 199−212.

(11) Milbradt, A. G.; Arthanari, H.; Takeuchi, K.; Boeszoermenyi, A.; Hagn, F.; Wagner, G. Increased resolution of aromatic cross peaks using alternate C-13 labeling and TROSY. *J. Biomol. NMR* **2015**, *62* (3), 291−301.

(12) Teilum, K.; Brath, U.; Lundström, P.; Akke, M. Biosynthetic C-13 labeling of aromatic side chains in proteins for NMR relaxation measurements. *J. Am. Chem. Soc.* **2006**, *128* (8), 2506−2507.

(13) Weininger, U. Site-selective 13C labeling of proteins using erythrose. *J. Biomol. NMR* **2017**, *67* (3), 191−200.

(14) Weininger, U. Optimal Isotope Labeling of Aromatic Amino Acid Side Chains for NMR Studies of Protein Dynamics. *Methods Enzymol* **2019**, *614*, 67−86.

(15) Raum, H. N.; Schorghuber, J.; Dreydoppel, M.; Lichtenecker, R. J.; Weininger, U. Site-selective (1)H/(2)H labeling enables artifact-free (1)H CPMG relaxation dispersion experiments in aromatic side chains. *J. Biomol NMR* **2019**, *73* (10−11), 633−639.

(16) Weininger, U.; Brath, U.; Modig, K.; Teilum, K.; Akke, M. Off-resonance rotating-frame relaxation dispersion experiment for C-13 in aromatic side chains using L-optimized TROSY-selection. *J. Biomol. NMR* **2014**, *59* (1), 23−29.

(17) Weininger, U.; Respondek, M.; Akke, M. Conformational exchange of aromatic side chains characterized by L-optimized TROSY-selected C-13 CPMG relaxation dispersion. *J. Biomol. NMR* **2012**, *54* (1), 9−14.

(18) Dreydoppel, M.; Lichtenecker, R. J.; Akke, M.; Weininger, U. 1)H R1rho relaxation dispersion experiments in aromatic side chains. *J. Biomol NMR* **2021**, *75*, 383.

(19) Dreydoppel, M.; Dorn, B.; Modig, K.; Akke, M.; Weininger, U. Transition-State Compressibility and Activation Volume of Transient Protein Conformational Fluctuations. *Jacs Au* **2021**, *1* (6), 833−842.

(20) Dreydoppel, M.; Raum, H. N.; Weininger, U. Slow ring flips in aromatic cluster of GB1 studied by aromatic C-13 relaxation dispersion methods. *J. Biomol. NMR* **2020**, *74* (2−3), 183−191.

(21) Weininger, U.; Modig, K.; Akke, M. Ring Flips Revisited: C-13 Relaxation Dispersion Measurements of Aromatic Side Chain Dynamics and Activation Barriers in Basic Pancreatic Trypsin Inhibitor. *Biochemistry* **2014**, *53* (28), 4519−4525.

(22) Weininger, U.; Respondek, M.; Löw, C.; Akke, M. Slow Aromatic Ring Flips Detected Despite Near-Degenerate NMR Frequencies of the Exchanging Nuclei. *J. Phys. Chem. B* **2013**, *117* (31), 9241−9247.

(23) Yang, C. J.; Takeda, M.; Terauchi, T.; Jee, J.; Kainosho, M. Differential Large-Amplitude Breathing Motions in the Interface of FKBP12-Drug Complexes. *Biochemistry* **2015**, *54* (47), 6983−6995.

(24) Kasinath, V.; Fu, Y. N.; Sharp, K. A.; Wand, A. J. A Sharp Thermal Transition of Fast Aromatic-Ring Dynamics in Ubiquitin. *Angew. Chem., Int. Ed.* **2015**, *54* (1), 102−7.

(25) Sathyamoorthy, B.; Singarapu, K. K.; Garcia, A. E.; Szyperski, T. Protein Conformational Space Populated in Solution Probed with Aromatic Residual Dipolar C-13-H-1 Couplings. *Chembiochem* **2013**, *14* (6), 684−688.

(26) Li, H.; Yamada, H.; Akasaka, K. Effect of pressure on the tertiary structure and dynamics of folded basic pancreatic trypsin inhibitor. *Biophys. J.* **1999**, *77* (5), 2801−2812.

(27) Wagner, G. Activation Volumes for the Rotational Motion of Interior Aromatic Rings in Globular-Proteins Determined by High-

Resolution H-1-Nmr at Variable Pressure. *FEBS Lett.* **1980**, *112* (2), 280−284.
(28) Wagner, G.; Bruhwiler, D.; Wüthrich, K. Reinvestigation of the Aromatic Side-Chains in the Basic Pancreatic Trypsin-Inhibitor by Heteronuclear Two-Dimensional Nuclear-Magnetic-Resonance. *J. Mol. Biol.* **1987**, *196* (1), 227−231.
(29) Igumenova, T. I.; Brath, U.; Akke, M.; Palmer, A. G. Characterization of chemical exchange using residual dipolar coupling. *J. Am. Chem. Soc.* **2007**, *129* (44), 13396.
(30) Vallurupalli, P.; Hansen, D. F.; Stollar, E.; Meirovitch, E.; Kay, L. E. Measurement of bond vector orientations in invisible excited states of proteins. *Proc. Natl. Acad. Sci. U. S. A.* **2007**, *104* (47), 18473−18477.
(31) Tjandra, N.; Bax, A. Direct measurement of distances and angles in biomolecules by NMR in a dilute liquid crystalline medium. *Science* **1997**, *278* (5340), 1111−4.
(32) Lindman, S.; Xue, W. F.; Szczepankiewicz, O.; Bauer, M. C.; Nilsson, H.; Linse, S. Salting the charged surface: pH and salt dependence of protein G B1 stability. *Biophys. J.* **2006**, *90* (8), 2911−21.
(33) Rückert, M.; Otting, G. Alignment of biological macromolecules in novel nonionic liquid crystalline media for NMR experiments. *J. Am. Chem. Soc.* **2000**, *122* (32), 7793−7797.
(34) Meissner, A.; Duus, J. O.; Sorensen, O. W. Spin-state-selective excitation. Application for E.COSY-type measurement of J(HH) coupling constants. *J. Magn. Reson.* **1997**, *128* (1), 92−97.
(35) Sorensen, M. D.; Meissner, A.; Sorensen, O. W. Spin-state-selective coherence transfer via intermediate states of two-spin coherence in IS spin systems: Application to E.COSY-type measurement of J coupling constants. *J. Biomol. NMR* **1997**, *10* (2), 181−186.
(36) Mulder, F. A. A.; de Graaf, R. A.; Kaptein, R.; Boelens, R. An off-resonance rotating frame relaxation experiment for the investigation of macromolecular dynamics using adiabatic rotations. *J. Magn. Reson.* **1998**, *131* (2), 351−357.
(37) Delaglio, F.; Grzesiek, S.; Vuister, G. W.; Zhu, G.; Pfeifer, J.; Bax, A. Nmrpipe - a Multidimensional Spectral Processing System Based on Unix Pipes. *J. Biomol. NMR* **1995**, *6* (3), 277−293.
(38) Ahlner, A.; Carlsson, M.; Jonsson, B. H.; Lundström, P. PINT: a software for integration of peak volumes and extraction of relaxation rates. *J. Biomol. NMR* **2013**, *56* (3), 191−202.
(39) Miloushev, V. Z.; Palmer, A. G. R(1p) relaxation for two-site chemical exchange: General approximations and some exact solutions. *J. Magn. Reson.* **2005**, *177* (2), 221−227.
(40) Press, W. H.; Teukolsky, S. A.; Vetterling, W. T.; Flannery, B. P.*Numerical Recipes in C++: The Art of Scientific Computing*, 2nd ed.; Cambridge University Press: Cambridge, 2002.
(41) Gallagher, T.; Alexander, P.; Bryan, P.; Gilliland, G. L. 2 Crystal-Structures of the B1 Immunoglobulin-Binding Domain of Streptococcal Protein-G and Comparison with Nmr. *Biochemistry* **1994**, *33* (15), 4721−4729.
(42) Franks, W. T.; Wylie, B. J.; Stellfox, S. A.; Rienstra, C. M. Backbone conformational constraints in a microcrystalline U-15N-labeled protein by 3D dipolar-shift solid-state NMR spectroscopy. *J. Am. Chem. Soc.* **2006**, *128* (10), 3154−5.
(43) Valafar, H.; Prestegard, J. H. REDCAT: a residual dipolar coupling analysis tool. *J. Magn. Reson.* **2004**, *167* (2), 228−241.
(44) Maciejewski, M. W.; Schuyler, A. D.; Gryk, M. R.; Moraru, I. I.; Romero, P. R.; Ulrich, E. L.; Eghbalnia, H. R.; Livny, M.; Delaglio, F.; Hoch, J. C. NMRbox: A Resource for Biomolecular NMR Computation. *Biophys. J.* **2017**, *112* (8), 1529−1534.
(45) Raum, H. N.; Dreydoppel, M.; Weininger, U. Conformational exchange of aromatic side chains by (1)H CPMG relaxation dispersion. *J. Biomol NMR* **2018**, *72* (1−2), 105−114.
(46) Rice, D. M.; Wittebort, R. J.; Griffin, R. G.; Meirovitch, E.; Stimson, E. R.; Meinwald, Y. C.; Freed, J. H.; Scheraga, H. A. Rotational Jumps of the Tyrosine Side-Chain in Crystalline Enkephalin - H-2 Nmr Line-Shapes for Aromatic Ring Motion in Solids. *J. Am. Chem. Soc.* **1981**, *103* (26), 7707−7710.
(47) Gauto, D. F.; Macek, P.; Barducci, A.; Fraga, H.; Hessel, A.; Terauchi, T.; Gajan, D.; Miyanoiri, Y.; Boisbouvier, J.; Lichtenecker, R.; Kainosho, M.; Schanda, P. Aromatic Ring Dynamics, Thermal Activation, and Transient Conformations of a 468 kDa Enzyme by Specific H-1-C-13 Labeling and Fast Magic-Angle Spinning NMR. *J. Am. Chem. Soc.* **2019**, *141* (28), 11183−11195.
(48) Paluch, P.; Pawlak, T.; Jeziorna, A.; Trebosc, J.; Hou, G. J.; Vega, A. J.; Amoureux, J. P.; Dracinsky, M.; Polenova, T.; Potrzebowski, M. J. Analysis of local molecular motions of aromatic sidechains in proteins by 2D and 3D fast MAS NMR spectroscopy and quantum mechanical calculations. *Phys. Chem. Chem. Phys.* **2015**, *17* (43), 28789−28801.
(49) Vugmeyster, L.; Ostrovsky, D.; Villafranca, T.; Sharp, J.; Xu, W.; Lipton, A. S.; Hoatson, G. L.; Vold, R. L. Dynamics of Hydrophobic Core Phenylalanine Residues Probed by Solid-State Deuteron NMR. *J. Phys. Chem. B* **2015**, *119* (47), 14892−904.
(50) Marino Perez, L.; Ielasi, F. S.; Bessa, L. M.; Maurin, D.; Kragelj, J.; Blackledge, M.; Salvi, N.; Bouvignies, G.; Palencia, A.; Jensen, M. R. Visualizing protein breathing motions associated with aromatic ring flipping. *Nature* **2022**, *602* (7898), 695−700.

https://doi.org/10.1021/acs.jpcb.2c05097
J. Phys. Chem. B 2022, 126, 7950−7956